mathematics

MDPI

Article

# Analysis of Magneto-hydrodynamics Flow and Heat Transfer of a Viscoelastic Fluid through Porous Medium in Wire Coating Analysis

**Zeeshan Khan [1,*], Muhammad Altaf Khan [2], Saeed Islam [2], Bilal Jan [1], Fawad Hussain [3], Haroon Ur Rasheed [1] and Waris Khan [4]**

1 Sarhad University of Science and Information Technology, Peshawar 25000, Pakistan; bilal.jan.bilal@gmail.com (B.J.); haroon.csit@suit.edu.pk (H.U.R)
2 Department1of Mathematics, Abdul Wali Khan University, Mardan 25000, Pakistan; altafdir@gmail.com (M.A.K); prof.saeed.uet@gmail.com (S.I.)
3 Department of Mathematics, Abbottabad University of Science and Technology, Abbottabad 25000, Pakistan; fawadhussain@yahoo.com
4 Department of Mathematics, Islamia College, Peshawar 25000, Pakistan; wariskhan758@yahoo.com
* Correspondence: zeeshansuit@gmail.com; Tel.: +92-302-554-2672

Received: 3 January 2017; Accepted: 6 May 2017; Published: 16 May 2017

**Abstract:** Wire coating process is a continuous extrusion process for primary insulation of conducting wires with molten polymers for mechanical strength and protection in aggressive environments. Nylon, polysulfide, low/high density polyethylene (LDPE/HDPE) and plastic polyvinyl chloride (PVC) are the common and important plastic resin used for wire coating. In the current study, wire coating is performed using viscoelastic third grade fluid in the presence of applied magnetic field and porous medium. The governing equations are first modeled and then solved analytically by utilizing the homotopy analysis method (HAM). The convergence of the series solution is established. A numerical technique called ND-solve method is used for comparison and found good agreement. The effect of pertinent parameters on the velocity field and temperature profile is shown with the help of graphs. It is observed that the velocity profiles increase as the value of viscoelastic third grade parameter $\beta$ increase and decrease as the magnetic parameter $M$ and permeability parameter $K$ increase. It is also observed that the temperature profiles increases as the Brinkman number $Br$, permeability parameter $K$, magnetic parameter $M$ and viscoelastic third grade parameter (non-Newtonian parameter) $\beta$ increase.

**Keywords:** magneto-hydrodynamics (MHD) flow; heat transfer; wire coating; Viscoelastic fluid; porosity; homotopy analysis method (HAM); ND-solve method

## 1. Introduction

Metallic coating is an industrial process for the supply of insulation, environmental safety, mechanical damage and protect against signal attenuation. The simple and appropriate process for wire coating is the coaxial extrusion process that operates at the maximum speed of pressure, temperature and wire drawing. This produces higher pressure in the particular region, resulting in a strong bond and rapid coating. Several studies have been focused on the co-extrusion process in which the fibers or wires are drawn inside the molten polymer filled in a die [1–4]. In coating of the wire, the rate of wire drawing, temperature and the quality of materials are important parameters. Different types of fluids are used for wire which depends upon the geometry of die, fluid viscosity, the temperature ofthe wire and that of the molten polymer. Considerable attention has been given to the Newtonian fluids to study the effect of heat transfer analysis. However, less attention has been given

to the non-Newtonian fluids [5–10]. A full review of the literature is beyond the scope of this work. However, some studies are listed here to provide a perspective of the work accomplished so far [11–18].

The properties of the final product greatly depend on the rate of cooling in the manufacturing processes. The central cooling system is beneficial to facilitate the process for a designed product. An electrically conducting polymeric liquid seems to be a good candidate for some industrial application such as in polymer technology and extrusion processes because the flow can be regulated by external means through a magnetic field as well as a porous matrix. Magneto-hydrodynamics (MHD) addresses the electrically conductiveffluid flowsiin the existenceoof a magneticffield. Researchers have devoted considerable attention to the study of MHD flow problems focusing on non-Newtonian fluids becauseoof its broad applicationsiin theffields of engineeringaand industrial manufacturing [19–22]. Some examples of these areas are energy generators MHD, melting of metals by the application of a magnetic field in an electric furnace, the cooling nuclear reactors, plasma studies, the use of non-metallic inclusions in theppurification of molten metals and extractions of geothermal energy [23–27]. The appliedmmagnetic field aswwell as porousmmatrix may playaan important roleiin controlling momentum andhheat transferiin the boundary layer flow of different fluids in the process of wire coating. In view of this, many authors have explored the effect of transverse magnetic field and porous matrix on Newtonian and non-Newtonian fluids. The effect of the transverse magnetic field as well as porosity were examined by several authors [28–32].

In the present article, we investigate the effect of MHD and heat transfer on the steady flow of viscoelastic fluid in which the wire has been drawn at higher speed in the presence of the porous medium. Although, there are a few studies on the flow and heat transfer of non-Newtonian fluids, careful examination of the literature reveals that a viscoelastic fluid has received very little attention. To the best of our knowledge, no one has studied MHD flow and heat transfer of a viscoelastic fluid for wire coating analysis in the presence of the porous medium. In this context, the constitutive equations for velocity and temperature profiles are solved by the homotopy analysis method (HAM) [33–41]. Furthermore, the ND-solve method is also applied for comparison [42].

## 2. Modeling of the Problem

Take an elasto-hydrodynamic coating system in which the continuum enters between the leakage control units that is attached to the melting chamber. The continuum after crossing the melting chamber enters the plasto-hydrodynamic pressure unit. Here, the hydrodynamic pressure helps to deposit a coating on the wire. The bull block after wounding a coated wire is driven by a variable speed motor as shown in Figure 1.

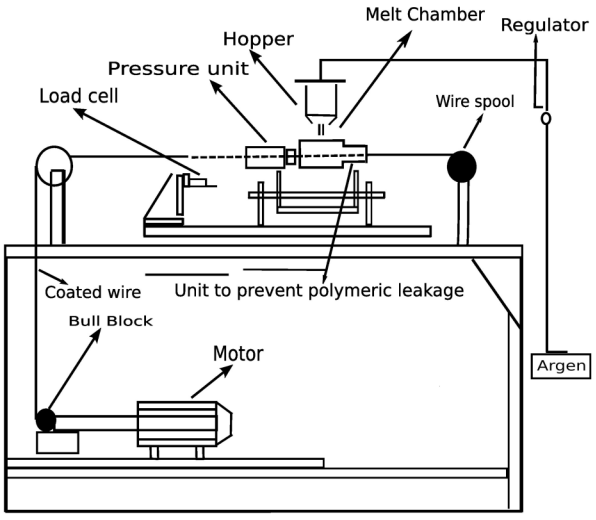


**Figure 1.** Typical wire coating line.

The schematic diagram of the flow geometry is shown in Figure 2. The wire is extruded along the central line of the die with velocity $V$ havingt temperature $\Theta_w$ and radius $R_w$ in a bath of third grade fluid used as a melt polymer like polyvinyl chloride (PVC) in a porous medium inside a stationary pressure type die of finite length $L$, radius $R_d$ and temperature $\Theta_d$. The fluid acts upon a constant pressure gradient in the axial direction and a transverse magnetic field of strength $B_0$. The magnetic field is perpendicular to the direction of incompressible flow. The magnetic Reynolds number is taken to be small enough so that the induced magnetic field can be neglected. As a result the Lorentz force comes into play in the present set up which affects the coating process.

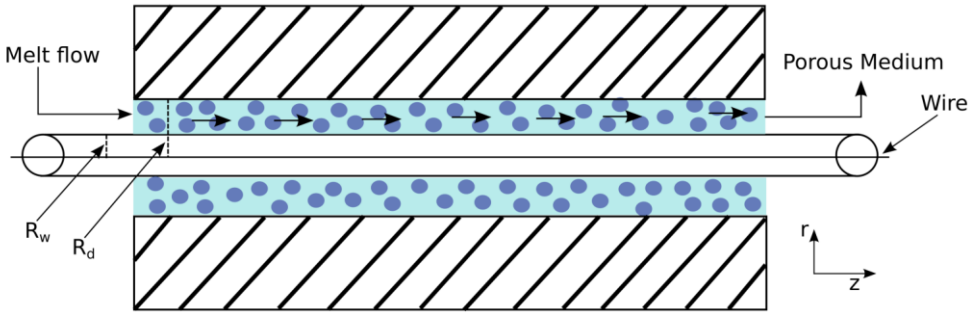


**Figure 2.** Wire coating process in a porous medium in a pressure type coating die.

The die is filled with an incompressible third grade fluid. The wire and die are concentric and the coordinate system is chosen at the center of the wire in which $r$ is taken perpendicular to the flow direction and $z$-axis is along the flow. The flow is considered steady, laminar and axisymmetric.

Furthermore, the design of the coating die is more important because it greatly affects the quality of the final product. For this reason, a pressure type coating die is considered for the wire coating process.

With the above mentioned frame of reference and assumptions the fluid velocity, extra stress tensor and temperature fields are considered as:

$$\vec{w} = [0, 0, u(r)],\ S = S(r),\ \Theta = \Theta(r) \tag{1}$$

Boundary conditions are:

$$\begin{aligned} u = V,\ \Theta = \Theta_w \text{ at } r = R_w, \\ u = 0,\ \Theta = \Theta_d \text{ at } r = R_d. \end{aligned} \tag{2}$$

The extra stress tensor for third grade fluid is defined as:

$$S = \eta A_1 + \alpha_1 A_2 + \alpha_2 A_1 + \tau_1 A_2 + \tau_2 (A_1 A_2 + A_2 A_1) + \tau_3 (tr A_2) A_1, \tag{3}$$

in which $\eta$, is the coefficient of1the viscosity1of the1fluid, $\alpha_1, \alpha_2, \tau_1, \tau_2, \tau_3$ are constant and $A_1, A_2, A_3$ are linekkinematic1tensors:

$$A_1 = L^T + L,\ A_n = A_{n-1} L^T + L A_{n-1} + \frac{D A_{n-1}}{Dt},\ n = 2, 3, \tag{4}$$

where $T$ denotes the transpose1of the matrix.

The governing equations for an incompressible fluid are [5–12,23]:

$$\nabla . \vec{w} = 0, \tag{5}$$

$$\rho \frac{D\vec{w}}{Dt} = -\vec{\nabla} p + \vec{F} + \vec{J} \times \vec{B} - \frac{\eta \vec{w}}{K}, \tag{6}$$

$$\rho c_p \frac{D\Theta}{Dt} = k \nabla^2 \Theta + \phi, \tag{7}$$

in which $\rho$, is the fluid density, $\frac{D}{Dt}$ the material derivative, $\overrightarrow{J}$ the current density, $\overrightarrow{B}$ the total magnetic field, $\eta$ the dynamic viscosity, $K$ the permeability parameter, $C_p$ the specific heat, $k$ the thermal conductivity, $\phi$ the dissipation function and $\overrightarrow{w}$ is the velocity vector.

In Equation (6), the body force $\overrightarrow{J} \times \overrightarrow{B}$ per unit volume of electromagnetic origin appears due to the interaction of the current and the magnetic field. The electrostatic force due to charge density is considered to be negligible. A uniform magnetic field of strength is assumed to be applied in the positive radial direction normal to the wire, i.e., the retarding force per unit volume acting along the $z$-axis is given by:

$$\overrightarrow{J} \times \overrightarrow{B} = (0, 0, -\sigma B_0^2 u). \tag{8}$$

In view of Equations (1)–(8) and assuming that there is no pressure gradient along the axial direction, we have the dimensional governing equation of the form:

$$2(\tau_2 + \tau_3)\frac{d}{dr}\left(r\left(\frac{du}{dr}\right)^3\right) + \frac{\eta}{r}\frac{d}{dr}\left(r\frac{du}{dr}\right) - \sigma B_0^2 u - \frac{\eta u}{K} = 0, \tag{9}$$

$$k\left(\frac{d^2\Theta}{dr^2} + \frac{1}{r}\frac{d\Theta}{dr}\right) + \eta\left(\frac{du}{dr}\right)^2 + 2(\tau_2 + \tau_3)\left(\frac{du}{dr}\right)^4 = 0, \tag{10}$$

We introduce the following dimensionless parameters:

$$\begin{gathered} r^* = \frac{r}{R_w}, u^* = \frac{u}{V}, \beta = \tau_2 + \tau_3, \frac{R_d}{R_w} = \delta > 1, \beta^* = \frac{\beta}{\eta\left(\frac{R_w^2}{V^2}\right)}, M^2 = \frac{\sigma B_0^2 R_w}{\eta}, \\ K = \frac{R_w^2}{VK^*}, \Theta = \frac{\Theta - \Theta_w}{\Theta_d - \Theta_w}, Br = \frac{\eta V^2}{k(\Theta_d - \Theta_w)}. \end{gathered} \tag{11}$$

In view of Equation (11), the Equations (2), (9) and (10) become:

$$r\frac{d^2u}{dr^2} + \frac{du}{dr} + 2\beta\left(3r\frac{d^2u}{dr^2}\left(\frac{du}{dr}\right)^2 + \left(\frac{du}{dr}\right)^3\right) - \left(M^2 + K\right)ur = 0, \tag{12}$$

$$\frac{d^2\Theta}{dr^2} + \frac{1}{r}\frac{d\Theta}{dr} + Br\left(\frac{du}{dr}\right)^2 + 2Br\beta\left(\frac{du}{dr}\right)^4 = 0, \tag{13}$$

$$u(1) = 1,\ u(\delta) = 0, \Theta(1) = 0,\ \Theta(\delta) = 1. \tag{14}$$

## 3. Solution by Homotopy Asymptotic Method

In order to solve Equations (12) and (13) under the boundary conditions (14) respectively, we use the HAM with the following procedure. The solutions having the auxiliary parameters $\hbar$ regulate and control the convergence of the solutions.

The initial guesses are selected as follows:

$$u_0(r) = \frac{-r + \delta}{-1 + \delta} \text{ and } \theta_0(r) = \frac{r - 1}{-1 + \delta}. \tag{15}$$

The linear operators are defined as:

$$L_u(u) = u'' \text{ and } \mathrm{L}_\theta(\theta) = \theta'' \ , \tag{16}$$

which have the following properties:

$$L_u(c_1 + c_2 r) = 0 \text{ and } \mathrm{L}_\theta(c_3 + c_4 r) = 0 \ , \tag{17}$$

where $c_i (i = 1 - 4)$ are the constants in general solution:

The resultant non-linear operatives are given as:

$$\begin{aligned} N_u[u(r;p)] &= \frac{\partial^2 u(r;p)}{\partial r^2} + \frac{\partial u(r;p)}{\partial r} + 2\beta\left(3r\frac{\partial^2 u(r;p)}{\partial r^2}\left(\frac{\partial u(r;p)}{\partial r}\right)^2 + \left(\frac{\partial u(r;p)}{\partial r}\right)^3\right) - (M^2+K)ur = 0, \\ N_\theta[u(r;p),\theta(r;p)] &= \left(\frac{\partial^2 \theta(r;p)}{\partial r^2} + \frac{1}{r}\frac{\partial \theta(r;p)}{\partial r}\right) + Br\left(\frac{\partial u(r;p)}{\partial r}\right)^2 + 2Br\beta\left(\frac{\partial u(r;p)}{\partial r}\right)^4. \end{aligned} \tag{18}$$

The basic idea of HAM is described in [33–41]; from Equations (12) and (13) are:

$$\begin{aligned} (1-p)L_u[u(r;p) - u_0(r)] &= p\hbar_u N_u[u(r;p)], \\ (1-p)L_\theta[\theta(r;p) - \theta_0(r)] &= p\hbar_\theta N_\theta[u(r;p),\theta(r;p)]. \end{aligned} \tag{19}$$

The boundary conditions are:

$$u(1;p) = 1,\ \theta(1;p) = 0, u(\delta;p) = 0,\ \theta(\delta;p) = 1, \tag{20}$$

where $p \in [0,1]$ is the imbedding parameter, and $\hbar_u$ and $\hbar_\theta$ are used to control the convergence of the solution. When $p = 0$ and $p = 1$ we have:

$$u(r;1) = u(r) \text{ and } \theta(r;1) = \theta(r). \tag{21}$$

Expanding $u(r;p)$ and $\theta(r;p)$ in Taylor's series about$p = 0$ and 1, we get:

$$u(r;p) = u_0(r) + \sum_{m=1}^{\infty} u_m(r)p^m, \theta(r;p) = \theta_0(r) + \sum_{m=1}^{\infty} \theta_m(r)p^m. \tag{22}$$

$$u(r) = u_0(r) + \sum_{m=1}^{\infty} u_m(r), \theta(r) = \theta_0(r) + \sum_{m=1}^{\infty} \theta_m(r). \tag{23}$$

where $u_m(r) = \frac{1}{m!}\frac{\partial u(r;p)}{\partial r}\Big|_{p=0}$ and $\theta_m(r) = \frac{1}{m!}\frac{\partial \theta(r;p)}{\partial r}\Big|_{p=0}$.

The $m$th-order problem satisfies the following:

$$L_u[u_m(r) - \chi_m u_{m-1}(r)] = \hbar_u R_m^u(r), L_\theta[\theta_m(r) - \chi_m \theta_{m-1}(r)] = \hbar_\theta R_m^\theta(r). \tag{24}$$

The corresponding boundary conditions are:

$$u_m(1) = u_m(\delta) = 0, \theta_m(1) = \theta_m(\delta) = 0. \tag{25}$$

here:

$$\begin{aligned} R_m^u(r) = r\frac{d^2u_{m-1}}{dr^2} + \frac{du_{m-1}}{dr} - (M^2+K)ru_{m-1} + 6\beta r\sum_{k=0}^{m-1}\sum_{i=0}^{k}\frac{du_{m-1-k}}{dr}\frac{du_{k-i}}{dr}\left[\frac{d^2u_{m-1}}{dr^2}\right] \\ +2\beta\sum_{k=0}^{m-1}\sum_{i=0}^{k}\sum_{j=0}^{i}\frac{du_{m-1-k}}{dr}\frac{du_{k-i}}{dr}\frac{du_{i-j}}{dr}, \end{aligned} \tag{26}$$

$$R_m^\theta(r) = r\frac{d^2\theta_{m-1}}{dr^2} + \frac{d\theta_{m-1}}{dr} + rBr\sum_{k=0}^{m-1}\sum_{i=0}^{k}\frac{du_{m-1-k}}{dr}\frac{du_{k-i}}{dr} + 2r\beta Br\sum_{k=0}^{m-1}\sum_{i=0}^{k}\sum_{j=0}^{i}\sum_{l=0}^{j}\frac{du_{m-1-k}}{dr}\frac{du_{k-i}}{dr}\frac{du_{i-j}}{dr}\frac{du_{j-l}}{dr}, \tag{27}$$

where $\chi_m = \begin{cases} 0, \text{ if } p \le 1 \\ 1, \text{ if } p > 1 \end{cases}$

The linear non-homogeneous problems (24) can be solved by using any symbolic computational software such as MATHEMATICAc (Wolfram Research Mathematica.v9.0.0.0 Incl Keymaker-AGAiN, Champaign, IL, USA) in the order $m$ = 1, 2, 3...

## 4. Results and Discussion

The Equation (23) give the series solution of the problem. The auxiliary parameter gives the convergence region. According to Liao [34] the appropriate region for the auxiliary parameter is the horizontal line. In Figure 3 $\hbar -$ curve is plotted for 30th order of approximation for velocity and temperature profiles. Figure 3 clearly shows the range for admissible values are $-1.5 \leq \hbar_u \leq -0.3$ and $-1.7 \leq \hbar_\Theta \leq -0.3$, respectively. The results using the pade-approximation are shown in Tables 1 and 2. From these tables, it is clear that the pade-approximation accelerates the convergence of the series solutions. Furthermore, the proposed method is also compared with ND-solve and Adomian decomposition method (ADM) as shown in Figure 4 and Table 3, and an outstanding correspondence is seen to exist between the two sets of data. The effect of non-Newtonian parameter of third grade parameter $\beta$, magnetic parameter $M$, permeability parameter $K$ and Brinkman number $Br$ on the velocity and temperature profiles are shown graphically in Figures 5–11 in the range $0 \leq \beta \leq 1.8, 0 \leq M \leq 1.5, 0 \leq K \leq 7$ and $1 \leq Br \leq 4$, respectively. Figure 5 shows the effect of viscoelastic third grade parameter (non-Newtonian parameter) $\beta$ on the velocity profile. It is observed that the velocity of the fluid increases with the increasing values of non-Newtonian third grade parameter. Figure 6 is sketched to see the effect of magnetic parameter $M$ on the velocity profile. Form Figure 6 it is noticed that the magnetic parameter $M$ has a decelerating effect on the velocity profile, i.e., increase in magnetic field strength contributes to slow down the velocity in the entire flow domain. It is observed that the magnetic field has a decelerating effect on the velocity field due to resistive Lorentz's force which comes into play as a resulting of the interaction of the magnetic field with conducting fluid, used as a coating material. It is also interesting to note that an increase in the non-Newtonian parameter, keeping the magnetic field strength fixed, leads to increase the velocity at all points of the flow domain. Thus, it is concluded that magnetic field contributes to slowing down the velocity whereas the non-Newtonian parameter characterizing the melt polymer (third grade fluid) accelerates it. As the velocity of coating fluid is an important design requirement, magnetic field strength and non-Newtonian characteristics of the fluid may be used as controlling devices for the required quality. Figure 7 shows the velocity variation for various values of permeability parameter $K$. It reveals as the permeability parameter increases, the velocity profile decreases. Figures 8–11 show the effect of Brinkman number $Br$, permeability parameter $K$, Magnetic parameter $M$ and non-Newtonian parameter $\beta$ on the temperature distribution respectively. Figure 8 shows the effect of Brinkman number $Br$ on the temperature profile. It is seen that as the Brinkman number increases, the temperature profile increases significantly at all points. Hence, it is observed that in the process of wire coating the Brinkman number, the relative measure of viscous heating with conducted heat, the temperature significantly accelerates at all points. The effect of permeability parameter $K$ on the temperature profile is shown in Figures 9 and 10 for small and large values respectively. From Figure 9 it is observed that for small values of permeability parameter $K$, i.e., in the domain [0, 1] it has no remarkable contribution. However, in the domain [1, 7] a two layer temperature distribution is observed. Temperature distribution increases in the domain $1 \leq r \leq 1.4$, then it decreases, as shown in Figure 10. The effect of magnetic parameter $M$ and non-Newtonian parameter $\beta$ on the temperature profile is shown in Figures 11 and 12 respectively. From Figure 11, it is observed that the temperature profile increases in the region $1 \leq r \leq 1.4$ and afterwards the reverse effect is observed. This may be attributed to the boundary surface effects which override the effect of the magnetic field. Figure 12 shows that the non-Newtonian parameter $\beta$ enhances the temperature profiles in the presence of porous matrix.

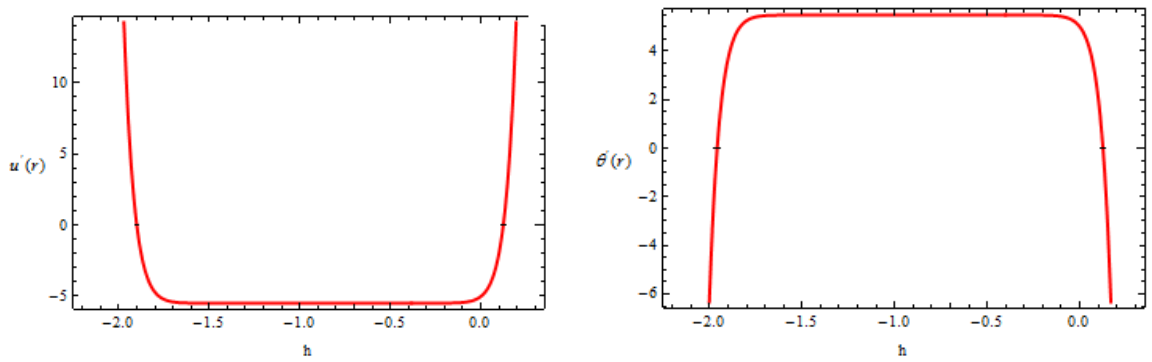


(**a**) (**b**)

**Figure 3.** The $\hbar-$ curve of velocity and temperature profiles for 20th-order approximation: (**a**) velocity; and (**b**) temperature.

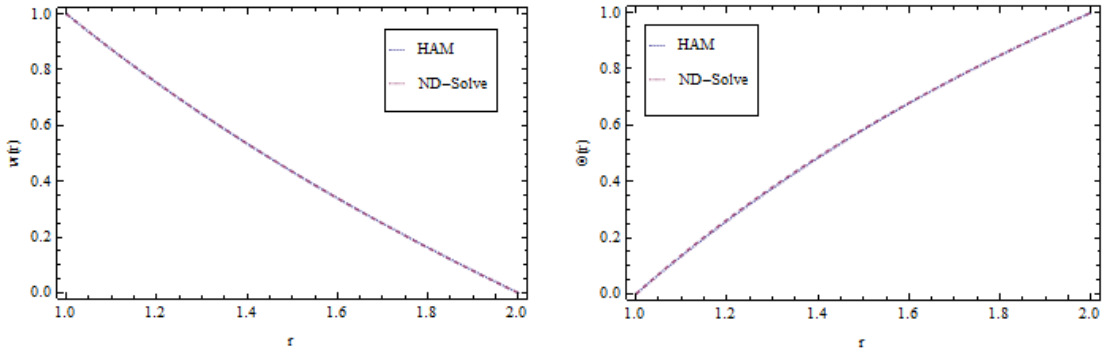


(**a**) (**b**)

**Figure 4.** Velocity and temperature comparison of homotopy analysis method (HAM) and ND-sole methods: (**a**) velocity; and (**b**) temperature.

**Table 1.** The homotopy-pade approximation of $u(r)$ and $\theta(r)$ for $\beta = 0.2,\ \delta = 2,\ K = 0.1,\ M = 0.2$.

| $r$ | $u(r)$ | $\theta(r)$ |
|---|---|---|
| [2/2] | −0.451024 | −0.654021 |
| [3/3] | −0.452521 | −0.653145 |
| [4/4] | −0.452365 | −0.653541 |
| [5/5] | −0.452630 | −0.653640 |
| [6/6] | −0.452315 | −0.654612 |
| [7/7] | −0.452001 | −0.654441 |

**Table 2.** The homotopy-pade approximation of $u(r)$ and $\theta(r)$ for $\beta = 0.4,\ \delta = 2,\ K = 0.2,\ M = 0.5$.

| $r$ | $u(r)$ | $\theta(r)$ |
|---|---|---|
| [2/2] | −0.7624392 | −0.663219 |
| [3/3] | −0.7621111 | −0.6639111 |
| [4/4] | −0.7636667 | −0.6646667 |
| [5/5] | −0.7633333 | −0.6645953 |
| [6/6] | −0.7621012 | −0.6634444 |
| [7/7] | −0.7621142 | −0.6633568 |

**Table 3.** Numerical comparison of HAM, ND-Sole Methods and Adomian decomposition method (ADM) for $\beta = 0.2,\ \delta = 2,\ K = 0.1,\ M = 0.2$.

| *r* | HAM | ND-Solve | ADM | Relative Error of HAM and ND-Solve |
|---|---|---|---|---|
| 1.0 | 1 | 1 | 1 | 0 |
| 1.2 | 0.66070791111 | 0.66070791111 | 0.66070791123 | $2.3 \times 10^{-9}$ |
| 1.4 | 0.41585866667 | 0.41585866667 | 0.41585866665 | $6.7 \times 10^{-9}$ |
| 1.6 | 0.23559573333 | 0.23559573333 | 0.23559573322 | $0.2 \times 10^{-10}$ |
| 1.8 | 0.10125404444 | 0.10125404444 | 0.10125404443 | $0.3 \times 10^{-10}$ |
| 2.0 | 0 | $1.17763568 \times 10^{-14}$ | $1.015426227 \times 10^{-13}$ | $0.012 \times 10^{-17}$ |

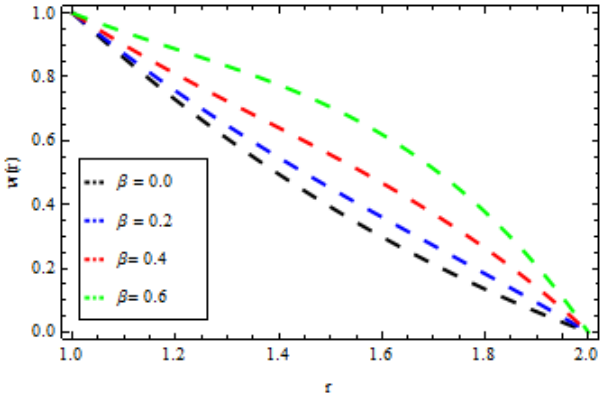


**Figure 5.** Velocity profile for various values of $\beta$ when $\delta = 2,\ K = 0.1,\ M = 0.2$.

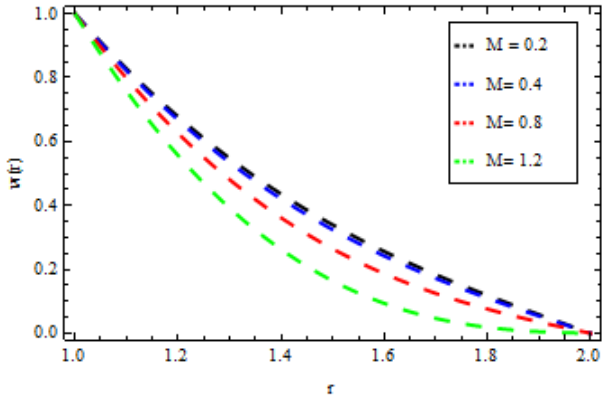


**Figure 6.** Velocity profile for various values of $M$ when $\delta = 2,\ K = 0.1,\ \beta = 0.2$.

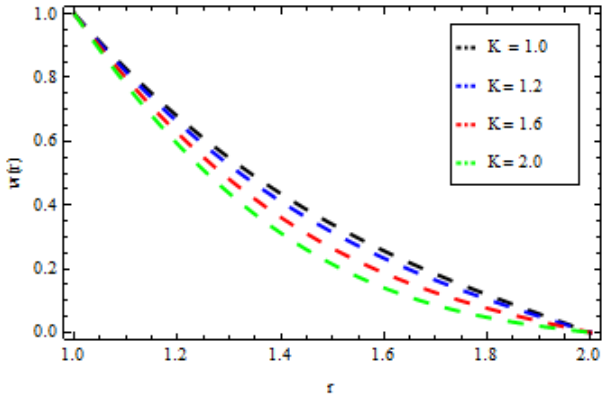


**Figure 7.** Velocity profile for various values of $K$ when $\delta = 2,\ \beta = 0.2,\ M = 0.2$.

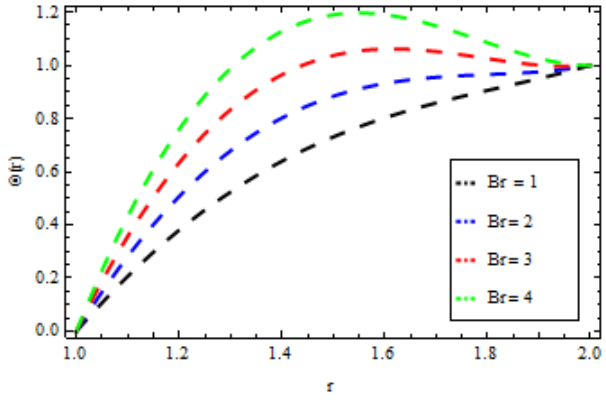


**Figure 8.** Temperature profile for various values of $Br$ when $\delta = 2,\ \beta = 0.2,\ M = 0.2,\ K = 0.1$.

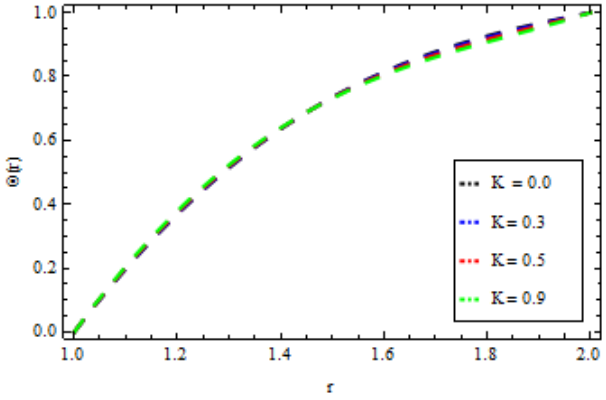


**Figure 9.** Temperature profile for various values of $K$ when $\delta = 2,\ \beta = 0.2,\ M = 0.2,\ Br = 1$.

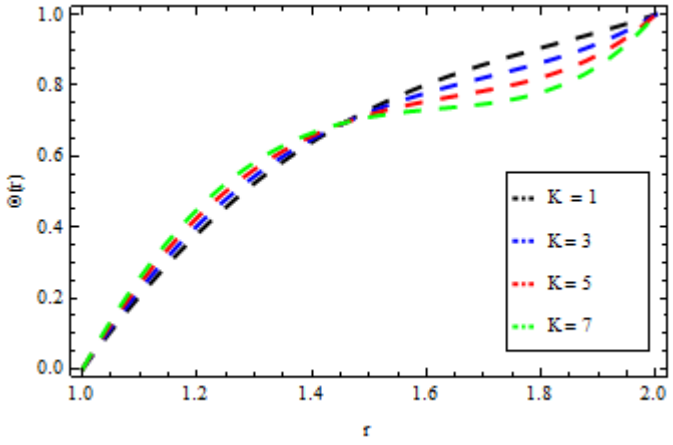


**Figure 10.** Temperature profile for various values of $K$ when$\delta = 2,\ \beta = 0.2,\ M = 0.2,\ Br = 1$.

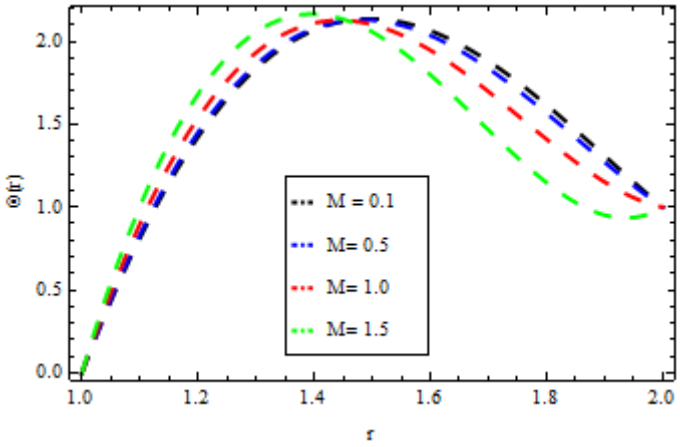


**Figure 11.** Temperature profile for various values of $M$ when $\delta = 2,\ \beta = 0.2,\ K = 0.2,\ Br = 1$.

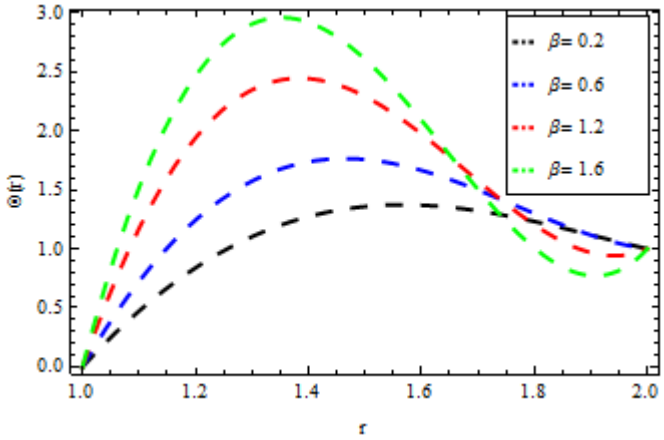


**Figure 12.** Temperature profile for various values of $\beta$ when $\delta = 2,\ K = 0.2,\ M = 0.2,\ Br = 1$.

## 5. Conclusions

In this study, the wire coating analysis is performed using viscoelastic third grade fluid as a melt polymer in a pressure type coating die. The expression for the velocity and temperature profiles are obtained analytically by HAM. The convergence of the series solution is established. The analytical results are also verified by utilizing the numerical technique so called ND-solve method. From both methods, the same solution is obtained. The effect of various parameters on the solutions are presented graphically. It is observed that the velocity profiles increase with the increasing value of viscoelastic third grade parameter $\beta$ and decrease with increasing the magnetic parameter $M$ and permeability parameter $K$. It is also observed that the temperature profiles increases when the Brinkman number $Br$, permeability parameter $K$, magnetic parameter $M$ and viscoelastic third grade parameter (non-Newtonian parameter) $\beta$ increase.

**Author Contributions:** Zeeshan Khanand, Muhammad Altaf Khan conceived and designed the experiments; Zeeshan Khan, Bilal Jan and Fawad Hussain performed the experiments; Zeeshan Khan, Haroon Ur Rasheed and Waris Khan analyzed the data; Zeeshan Khan and Muhammad Altaf Khan contributed reagents/materials/analysis tools; Zeeshan Khan wrote the paper, Muhammad Altaf Khan and Saeed Islam revised the manuscript.

**Conflicts of Interest:** The authors declare no conflict of interest.

## References

1. Han, C.D.; Rao, D. The rheology of wire coating extrusion. *Polym. Eng. Sci.* **1978**, *18*, 1019–1029. [CrossRef]

2. Nayak, M.K. *Wire Coating Analysis*, 2nd ed.; India Tech: New Delhi, Indina, 2015.
3. Caswell, B.; Tanner, R.J. Wire coating die using finite element methods. *Polym. Eng. Sci.* **1978**, *18*, 417–421. [CrossRef]
4. Tucker, C.L. *Computer Modeling for Polymer Processing*; Hanser: Munich, Germany, 1989; pp. 311–317.
5. Akter, S.; Hashmi, M.S.J. Analysis of polymer flow in a canonical coating unit: Power law approach. *Prog. Org. Coat.* **1999**, *37*, 15–22. [CrossRef]
6. Akter, S.; Hashmi, M.S.J. Plasto-hydrodynamic pressure distribution in a tepered geometry wire coating unit. In Proceedings of the 14th Conference of the Irish manufacturing committee (IMC14), Dublin, Ireland, 3–5 September 1997; pp. 331–340.
7. Siddiqui, A.M.; Haroon, T.; Khan, H. Wire coating extrusion in a Pressure-type Die in the flow of a third grade fluid. *Int. J. Non-Linear Sci. Numeric. Simul.* **2009**, *10*, 247–257.
8. Fenner, R.T.; Williams, J.G. Analytical methods of wire coating die design. *Trans. Plast. Inst.* **1967**, *35*, 701–706.
9. Shah, R.A.; Islam, S.; Siddiqui, A.M.; Haroon, T. Optimal homotopy asymptotic method solution of unsteady second grade fluid in wire coating analysis. *J. Ksiam* **2011**, *15*, 201–222.
10. Shah, R.A.; Islam, S.; Siddiqui, A.M.; Haroon, T. Exact solution of differential equation arising in the wire coating analysis of an unsteady second grad fluid. *Math. Comp. Mod.* **2013**, *57*, 1284–1288. [CrossRef]
11. Mitsoulis, E. Fluid flow and heat transfer in wire coating. *Adv. Polym. Technol.* **1986**, *6*, 467–487. [CrossRef]
12. Oliveira, P.J.; Pinho, F.T. Analytical solution for fully developed channel and pipe flow of Phan-Thien, Tanner fluids. *J. Fluid Mech.* **1999**, *387*, 271–280. [CrossRef]
13. Thien, N.P.; Tanner, R.I. A new constitutive equation derived from network theory. *J. Non-Newtonian Fluid Mech.* **1977**, *2*, 353–365. [CrossRef]
14. Kasajima, M.; Ito, K. Post-treatment of Polymer extrudate in wire coating. *Appl. Polym. Symp.* **1973**, *20*, 221–235.
15. Wagner, R.; Mitsoulis, E. Effect of die design on the analysis of wire coating. *Adv. Polym. Technol.* **1985**, *5*, 305–325. [CrossRef]
16. Bagley, E.B.; Storey, S.H. Wire and wire ccoating product. *Int. J. Polym. Sci.* **1963**, *38*, 1104–1122.
17. Pinho, F.T.; Oliveira, P.J. Analysis of forced convection in pipes and channels with simplified Phan-Thien-Tanner fluid. *Int. J. Heat Mass Transf.* **2000**, *43*, 2273–2287. [CrossRef]
18. Shah, R.A.; Islam, S.; Siddiqui, A.M.; Haroon, T. Wire coating analysis with Oldroyd 8-constant fluid by optimal homotopy asymptotic method. *Comput. Math. Appl.* **2012**, *63*, 695–707. [CrossRef]
19. Abel, S.; Prasad, K.V.; Mahaboob, A. Buoyancy force and thermal radiation effects in MHD boundary layer viscoelastic fluid flow over continuously moving stretching surface. *Int. J. Therm. Sci.* **2005**, *44*, 465–476. [CrossRef]
20. Sarpakaya, T. Flow of non-Newtonian fluids in a magnetic field. *AIChE J.* **1961**, *7*, 324–328. [CrossRef]
21. Abel, M.S.; Shinde, J.N. The effects of MHD flow and heat transfer for the UCM fluid over a stretching surface in presence of thermal radiation. *Adv. Math. Phys.* **2015**, *2012*, 21. [CrossRef]
22. Chen, V.C. On the analytical solution of MHD flow and heat transfer for two types of viscoelastic fluid over a stretching sheet with energy dissipation, internal heat source and thermal radiation. *Int. J. Heat Mass Transf.* **2010**, *19*, 4264–4273. [CrossRef]
23. Hayat, T.; Sajid, M. Homotopy analysis of MHD boundary layer flow of an upper-convected Maxwell fluid. *Int. J. Eng. Sci.* **2007**, *45*, 393–401. [CrossRef]
24. Wang, Y.; Hayat, T. Fluctuating flow of a Maxwell fluid past a porous plate with variable suction, Nonlinear Analysis. *Real World Appl.* **2008**, *9*, 1269–1282. [CrossRef]
25. Rashidi, S.; Dehghan, M. Study of stream wise transverse magnetic fluid flow with heat transfer around an obstacle embedded in a porous medium. *J. Magn. Magn. Mater.* **2015**, *378*, 128–137. [CrossRef]
26. Ellahi, R.; Rahman, S.U.; Nadeem, S.; Vafai, K. The blood flow of Prandtl fluid through a tapered stenosed arteries in permeable walls with magnetic field. *Commun. Theor. Phys.* **2015**, *63*, 353–358. [CrossRef]
27. Kandelousi, M.S.; Ellahi, R. Simulation of ferrofluid flow for magnetic drug targeting using the lattice Boltzmann method. *Z. Naturf. A* **2015**, *70*, 115–124. [CrossRef]
28. Nayak, M.K. Chemical reaction effect on MHD viscoelastic fluid over a stretching sheet through porous medium. *Mecanica* **2016**, *51*, 1699–1711. [CrossRef]
29. Vafai, K. *Handbook of Porous Media*, 2nd ed.; Taylor and Francis: New York, NY, USA, 2015.
30. Nield, I.A.; Bejan, A. *Cpvection in Porou Media*, 4th ed.; Springer: New York, NY, USA, 2012.

31. Daniel, Y.S. Steady MHD laminar flows and heat transfer adjacent to porous stretching sheet using HAM. *Am. J. Heat Mass Transf.* **2015**, *2*, 146–159. [CrossRef]
32. Nayak, M.K. *Flow through Porous Median*, 1st ed.; India Tech: New Delhi, India, 1989.
33. Liao, S.J. An analytic solution of unsteady boundary layer flows caused by an impulsively stretching plate. *Commun. Nonlinear Sci. Numer Simul.* **2006**, *11*, 326–339. [CrossRef]
34. Liao, S.J. A new branch of solutions of boundary layer flows over a permeable stretching plate. *Int. J. Nonlinear Mech.* **2007**, *42*, 819–830. [CrossRef]
35. Liao, S.J. Beyond perturbation: review on the basic ideas of homotopy analysis method and its application. *Adv. Mech.* **2008**, *38*, 1–34.
36. Abbasbandy, S. The application of homotopy analysis method to nonlinear equations arising in heat transfer. *Phys. Lett. A* **2006**, *360*, 109–113. [CrossRef]
37. Abbasbandy, S. Homotopy analysis method for heat radiation equation. *Int. Commun. Heat Mass Transf.* **2007**, *34*, 380–387. [CrossRef]
38. Hayat, T.; Khan, M.; Ayub, M. On the explicit analytic solutions of an Oldroyd 6-constant fluid. *Int. J. Eng. Sci.* **2004**, *42*, 123–135. [CrossRef]
39. Hayat, T.; Khan, M.; Asghar, S. Homotopy analysis of MHD flows of an Oldroyd 6-constant fluid. *Acta Mech.* **2004**, *168*, 213–232. [CrossRef]
40. Khan, M.; Abbas, Z.; Hayat, T. Analytic solution for the flow of Sisko fluid through a porous medium. *Transp. Porous Media* **2008**, *71*, 23–37. [CrossRef]
41. Abbas, Z.; Sajid, M.; Hayat, T. MHD boundary layer flow of an upper-convected Maxwell fluid in porous channel. *Theor. Comput. Fluid Dyn.* **2006**, *20*, 229–238. [CrossRef]
42. Khan, W.; Gul, T.; Idrees, M.; Islam, S.; Khan, I.; Dennis, L.C.C. Thin Film Williamson Nanofluid Flow with Varying Viscosity and Thermal Conductivity on a Time-Dependent Stretching Sheet. *Appl. Sci.* **2016**, *6*. [CrossRef]